TABLE 1 Measured Distances for Multiple Targets

Real Distance (cm)	Measured Distance to the Target B (cm)	Measurement Error (%)
50.0	47.51	4.98
60.0	58.79	2.02
70.0	65.3	6.7
	69.19 (Removing the target A)	1.16
90.	94.1	4.56

power detectors is demonstrated via distance measurements to a single target and multiple targets. The RF power detector is designed with a dummy structure and a differential common emitter amplifier to cancel DC offset voltage. The maximum distance errors are 2% in a single target and 6.7% in multitarget environment using traveling wave antennas. The radar sensor has high-range accuracy with narrow bandwidth. The sensor for short-range detection has the advantages of easy designs to the all components in the sensor and high-range accuracy from zero to the maximum detectable range. The whole size of the radar sensor module included the six-port network made by HBT MMIC process, a signal conditioning block, and a patch antenna is $4 \times 4 \times 2$ cm^3.

REFERENCES

1. G.F. Engen, The six-port reflectometer: An alternative network analyzer, IEEE Trans Microwave Theory Tech MTT-25 (1977), 1077–1079.
2. C.G. Miguélez, A new automobile radar based on the six-port phase/frequency discriminator, IEEE Trans Vehicular Technol 49 (2000), 1416–1423.
3. J. Wenger, Automotive radar—status and perspectives, IEEE CSIC Digest (2005), 21–24.
4. V. Giammello, E. Ragonese, and G. Palmisano, A 24/77-GHz SiGe BiCMOS transmitter chipset for automotive radar, Microwave Opt Technol Lett 55 (2013), 782–786.
5. F. Zhenghe, L. Yang, L. Liwan, P. Weifeng, and C. Yaqin, Requirement analysis of linearity for FMCW source using open-loop correction, In: Proceedings of International Conference on Microwave Millimeter Wave Technology, 2000, pp. 679–682.
6. R.G. Meyer, Low-power monolithic RF peak detector analysis, IEEE J Solid-State Circuits 30 (1995), 65–67.
7. J.-R. Yang, D.-W. Kim, and S. Hong, A calibration method of a range finder with a six-port network, IEEE Microwave Compon Lett 17 (2007), 549–551.
8. J.R. James and P.S. Hall, Handbook of microstrip antennas, IEE Electromagnetic Waves Series, London, UK, vol. 28, 1989.

STABILITY ANALYSIS OF THE PML SCHEME FOR CN-FDTD AND ADI-FDTD

Jiunn-Nan Hwang and Fu-Chiarng Chen
Department of Electrical Engineering, National Chiao Tung University, Hsinchu 300, Taiwan; Corresponding author: fchen@faculty.nctu.edu.tw

Received 14 March 2014

ABSTRACT: *The alternating direction implicit-finite-difference time-domain (ADI-FDTD) method can be seen as a second-order perturbation of the Crank–Nicolson FDTD (CN-FDTD) scheme. When the PML is introduced for the ADI-FDTD method, the perturbation term will affect the stability of the ADI-FDTD method. In this work, the stability analysis of the PML schemes for the ADI-FDTD and CN-FDTD are demonstrated. It is found that the PML equations for ADI-FDTD method will be unstable due to the perturbation term.* © 2014 Wiley Periodicals, Inc. Microwave Opt Technol Lett 56:2637–2642, 2014; View this article online at wileyonlinelibrary.com. DOI 10.1002/mop.28658

Key words: *Crank–Nicolson FDTD; alternating direction implicit-finite-difference time-domain; PML; stability; perturbation term*

1. INTRODUCTION

Finite-difference time-domain (FDTD) method has been widely used to analyze the electromagnetic problems [1]. Due to the explicit nature of this method, the time step size is restricted by the Courant, Friedrichs, and Lewy (CFL) stability condition. A stable alternating direction implicit (ADI) scheme was introduced for the FDTD method. The ADI-FDTD method is an attractive method due to its unconditional stability with large CFL number (CFLN) [2, 3]. When the ADI-FDTD method is used to simulate unbounded region problems, efficient absorbing boundary conditions must be used. The PML schemes were used for the ADI-FDTD method [4–6]. In [7, 8], the ADI-FDTD with CFS PML was also proposed to reduce the reflection error. However, the implementation of the PML in the ADI-FDTD method can affect the stability of this scheme. In [9], it is found that the ADI-FDTD method with split-field PML will lead to late-time instability. The Crank–Nicolson FDTD (CN-FDTD) is found to be another alternative unconditionally stable FDTD method. The ADI-FDTD can be seen as an approximation of the CN-FDTD scheme [10]. In [11, 12], the CN-FDTD with nearly PML and split-field PML were proposed. It is shown that the CN-FDTD can remain unconditionally stable with PML implementation.

In this article, the stability analysis of the PML schemes for the CN-FDTD and ADI-FDTD will be studied. The von Neumann analysis is used to determine the stability of these schemes. The difference between the CN-FDTD and ADI-FDTD is the Δt^2 perturbation term. From this study, it is found that the perturbation term will affect the stability of PML schemes for ADI-FDTD method.

2. PML FOR CN-FDTD AND ADI-FDTD

The ADI-FDTD can be seen as a second-order perturbation of CN-FDTD. Their formulations are described briefly. The Maxwell's curl equations are given by

$$\partial_t \vec{E} = \frac{1}{\varepsilon}\tilde{\Re}\vec{H} \quad \partial_t \vec{H} = -\frac{1}{\mu}\tilde{\Re}\vec{E} \tag{1}$$

where ε and μ are the permittivity and permeability, respectively. $\vec{E}$ and $\vec{H}$ are the electric and magnetic fields, and $\tilde{\Re}$ is the curl operator. One can replace all the derivatives by centered difference operator and average in time the field affected by the curl operator to derive the CN-FDTD scheme,

$$(\vec{\Psi}^{n+1} - \vec{\Psi}^{n}) = \tilde{\Re}_{\mathrm{T}} \frac{\Delta t}{2} (\vec{\Psi}^{n+1} + \vec{\Psi}^{n}) \tag{2}$$

where $\vec{\Psi} = (E_x \quad E_y \quad E_z \quad H_x \quad H_y \quad H_z)^{\mathrm{T}}$ is the numerical vector field and the operator $\tilde{\Re}_{\mathrm{T}}$ is the numerical counterpart of $\tilde{\Re}$.

Equation (2) is the CN-FDTD scheme. It will require large computational resources to solve this scheme. Nevertheless, the

CN-FDTD can be reformulated to ADI-FDTD scheme that can be solved efficiently. Based on [10], the CN-FDTD method can be split into two-step procedure for ADI-FDTD.

The space operator is $\tilde{\Re}_{\mathrm{T}}$ is decomposed as

$$\tilde{A}+\tilde{B}=\tilde{\Re}_{\mathrm{T}} \tag{3}$$

and (2) can be rewritten as

$$\left(\tilde{I}-\frac{\Delta t}{2}(\tilde{A}+\tilde{B})\right)\tilde{\Psi}^{n+1}=\left(\tilde{I}+\frac{\Delta t}{2}(\tilde{A}+\tilde{B})\right)\tilde{\Psi}^{n} \tag{4}$$

The CN-FDTD scheme (4) can be rewritten as

$$\begin{aligned}\left(\tilde{I}-\frac{\Delta t}{2}\tilde{A}\right)\left(\tilde{I}-\frac{\Delta t}{2}\tilde{B}\right)\vec{\Psi}^{n+1}&=\left(\tilde{I}+\frac{\Delta t}{2}\tilde{A}\right)\left(\tilde{I}+\frac{\Delta t}{2}\tilde{B}\right)\vec{\Psi}^{n}\\&+\frac{\Delta t^2}{4}\tilde{A}\tilde{B}(\vec{\Psi}^{n+1}-\vec{\Psi}^{n})\end{aligned} \tag{5}$$

If we neglect the Δt^2 perturbation term, we can get the approximation of CN-FDTD as ADI-FDTD

$$\left(\tilde{I}-\frac{\Delta t}{2}\tilde{A}\right)\left(\tilde{I}-\frac{\Delta t}{2}\tilde{B}\right)\vec{\Psi}^{n+1}=\left(\tilde{I}+\frac{\Delta t}{2}\tilde{A}\right)\left(\tilde{I}+\frac{\Delta t}{2}\tilde{B}\right)\vec{\Psi}^{n} \tag{6}$$

Therefore, the ADI-FDTD scheme (6) can be seen as a second-order perturbation of the CN-FDTD (2)

Equation (6) can be further split into two updating steps

$$\begin{aligned}\left(\tilde{I}-\frac{\Delta t}{2}\tilde{A}\right)\vec{\Psi}^{n*}&=\left(\tilde{I}+\frac{\Delta t}{2}\tilde{B}\right)\vec{\Psi}^{n},\\\left(\tilde{I}-\frac{\Delta t}{2}\tilde{B}\right)\vec{\Psi}^{n+1}&=\left(\tilde{I}+\frac{\Delta t}{2}\tilde{A}\right)\vec{\Psi}^{n*}\end{aligned} \tag{7}$$

where $\vec{\Psi}^{n*}$ is an auxiliary intermediate vector field. The ADI-FDTD Eq. (7) can be solved efficiently.

To simulate unbounded region problems, the PML formulations should be implemented for CN-FDTD and ADI-FDTD. We can use the same procedure to reformulate the PML equations. For the PML equations, the PML conductivity is incorporated into matrix $\tilde{\Re}_{\mathrm{T}}$. Once we derive the operator $\tilde{\Re}_{\mathrm{T}}$ and split into two operators $\tilde{A}$ and $\tilde{B}$, we can reformulate the PML equations for CN-FDTD and ADI-FDTD. In this study, the unsplit-field PML, split-field PML, and CFS PML formulations are investigated.

2.1. Unsplit-Field PML Scheme

The unsplit-field PML scheme is based on the formulations derived in [6]. The unsplit form PML equations are

$$\partial_t\vec{E}=\frac{1}{\varepsilon}\tilde{\Re}\vec{H}-\frac{1}{\varepsilon}\tilde{\sigma}_{\mathrm{o}}\vec{E}-\frac{1}{\varepsilon}(\tilde{\sigma}_{\mathrm{e}}-\tilde{\sigma}_{\mathrm{o}})\vec{E}_{\mathrm{e}} \tag{8a}$$

$$\partial_t\vec{H}=-\frac{1}{\mu}\tilde{\Re}\vec{E}-\frac{1}{\varepsilon}\tilde{\sigma}_{\mathrm{e}}\vec{H}-\frac{1}{\varepsilon}(\tilde{\sigma}_{\mathrm{e}}-\tilde{\sigma}_{\mathrm{o}})\vec{H}_{\mathrm{o}} \tag{8b}$$

$$\partial_t\vec{E}_{\mathrm{e}}=\frac{1}{\varepsilon}\tilde{\Re}_{\mathrm{e}}\vec{H}-\frac{1}{\varepsilon}\tilde{\sigma}_{\mathrm{e}}\vec{E}_{\mathrm{e}} \tag{8c}$$

$$\partial_t\vec{H}_{\mathrm{o}}=-\frac{1}{\mu}\tilde{\Re}_{\mathrm{o}}\vec{E}-\frac{1}{\varepsilon}\tilde{\sigma}_{\mathrm{o}}\vec{H}_{\mathrm{o}} \tag{8d}$$

where ∂_u represents the partial derivative with respective to u direction, $\vec{E}_{\mathrm{e}}$ and $\vec{H}_{\mathrm{o}}$ are two auxiliary fields, and

$$\begin{aligned}\tilde{\Re}&=\begin{pmatrix}0&-\partial_z&\partial_y\\\partial_z&0&-\partial_x\\-\partial_y&\partial_x&0\end{pmatrix},\quad \tilde{\Re}=\tilde{\Re}_{\mathrm{e}}+\tilde{\Re}_{\mathrm{o}}\\\tilde{\Re}_{\mathrm{e}}&=\begin{pmatrix}0&0&\partial_y\\\partial_z&0&0\\0&\partial_x&0\end{pmatrix}\quad \tilde{\Re}_{\mathrm{o}}=\begin{pmatrix}0&-\partial_z&\partial\\0&0&-\partial_x\\-\partial_y&0&0\end{pmatrix}\\\tilde{\sigma}_{\mathrm{e}}&=\begin{pmatrix}\sigma_y&0&0\\0&\sigma_z&0\\0&0&\sigma_x\end{pmatrix}\quad \tilde{\sigma}_{0}=\begin{pmatrix}\sigma_z&0&0\\0&\sigma_x&0\\0&0&\sigma_y\end{pmatrix}\end{aligned} \tag{9}$$

(8) can be written in a compact form as

$$\partial_t\vec{\Psi}(t)=\tilde{\Re}_{\mathrm{T}}\vec{\Psi}(t) \tag{10}$$

where $\Psi(t)$ is the compound Cartesian vector

$$\begin{aligned}\vec{\Psi}=(&E_x\quad E_y\quad E_z\quad H_x\quad H_y\quad H_z\\&E_{\mathrm{ex}}\quad E_{\mathrm{ey}}\quad E_{\mathrm{ez}}\quad H_{\mathrm{ox}}\quad H_{\mathrm{oy}}\quad H_{\mathrm{oz}})^{\mathrm{T}}\end{aligned} \tag{11}$$

And

$$\tilde{\Re}_{\mathrm{T}}=\begin{pmatrix}-\frac{1}{\varepsilon}\tilde{\sigma}_{\mathrm{o}}&\frac{1}{\varepsilon}\tilde{\Re}&-\frac{1}{\varepsilon}(\tilde{\sigma}_{\mathrm{e}}-\tilde{\sigma}_{\mathrm{o}})&\tilde{0}\\\frac{1}{\mu}\tilde{\Re}&-\frac{1}{\varepsilon}\tilde{\sigma}_{\mathrm{e}}&\tilde{0}&\frac{1}{\varepsilon}(\tilde{\sigma}_{\mathrm{e}}-\tilde{\sigma}_{\mathrm{o}})\\\tilde{0}&\frac{1}{\varepsilon}\tilde{\Re}_{\mathrm{e}}&-\frac{1}{\varepsilon}\tilde{\sigma}_{\mathrm{e}}&\tilde{0}\\-\frac{1}{\mu}\tilde{\Re}_{\mathrm{o}}&\tilde{0}&\tilde{0}&-\frac{1}{\varepsilon}\tilde{\sigma}_{\mathrm{o}}\end{pmatrix} \tag{12}$$

where $\tilde{I}$ and $\tilde{0}$ are 3×3 identity and null matrix, respectively.

The operators $\tilde{A}$ and $\tilde{B}$ are chosen, so that

$$\tilde{A}+\tilde{B}=\tilde{\Re}_{\mathrm{T}} \tag{13}$$

A possible choice of $\tilde{A}$ and $\tilde{B}$ is given by

$$\tilde{A}=\begin{pmatrix}\tilde{0}&\frac{1}{\varepsilon}\tilde{\Re}_{\mathrm{e}}&-\frac{1}{\varepsilon}\tilde{\sigma}_{\mathrm{e}}&\tilde{0}\\-\frac{1}{\mu}\tilde{\Re}_{\mathrm{o}}&\tilde{0}&\tilde{0}&-\frac{1}{\varepsilon}\tilde{\sigma}_{\mathrm{o}}\\\tilde{0}&\frac{1}{\varepsilon}\tilde{\Re}_{\mathrm{e}}&-\frac{1}{\varepsilon}\tilde{\sigma}_{\mathrm{e}}&\tilde{0}\\-\frac{1}{\mu}\tilde{\Re}_{\mathrm{o}}&\tilde{0}&\tilde{0}&-\frac{1}{\varepsilon}\tilde{\sigma}_{\mathrm{o}}\end{pmatrix} \tag{14}$$

$$\tilde{B}=\begin{pmatrix} -\frac{1}{\varepsilon}\tilde{\sigma}_{\mathrm{o}} & \frac{1}{\varepsilon}\tilde{\Re}_{\mathrm{o}} & \frac{1}{\varepsilon}\tilde{\sigma}_{\mathrm{o}} & \tilde{0} \\ -\frac{1}{\mu}\tilde{\Re}_{\mathrm{e}} & -\frac{1}{\varepsilon}\sigma_{\mathrm{e}} & \tilde{0} & \frac{1}{\varepsilon}\tilde{\sigma}_{\mathrm{e}} \\ \tilde{0} & \tilde{0} & \tilde{0} & \tilde{0} \\ \tilde{0} & \tilde{0} & \tilde{0} & \tilde{0} \end{pmatrix} \tag{15}$$

The field components $\overrightarrow{E}$, $\overrightarrow{H}$, $\overrightarrow{E}_{\mathrm{e}}$, and $\overrightarrow{H}_{\mathrm{o}}$ can be solved by CN-FDTD (4) or by two updating steps ADI-FDTD method (7). The system Eq. (7) can be further triangularized to solve it. When we set the PML conductivity $\sigma_x = \sigma_y = \sigma_z = 0$, $\overrightarrow{E}$ and $\overrightarrow{H}$ formulations will be identical to the ADI-FDTD method.

2.2. Split-Field PML Scheme

The split-field PML formulations can also be expressed in the partial differential form (1) and solved by the CN-FDTD scheme. Based on [4], the field vector is defined as

$$\overrightarrow{\Psi}=(E_{xy}\quad E_{yz}\quad E_{zx}\quad E_{xz}\quad E_{yx}\quad E_{zy}\quad H_{xy}\quad H_{yz}\quad H_{zx}\quad H_{xz}\quad H_{yx}\quad H_{zy})^{\mathrm{T}} \tag{16}$$

and $\tilde{\Re}_{\mathrm{T}}$ is a 12×12 dimensional space operator

$$\tilde{\Re}_{\mathrm{T}}=\begin{pmatrix} -\frac{1}{\varepsilon}\tilde{\sigma}_{\mathrm{e}} & \tilde{0} & \frac{1}{\varepsilon}\tilde{R}_{\mathrm{e}} & \frac{1}{\varepsilon}\tilde{R}_{\mathrm{e}} \\ \tilde{0} & -\frac{1}{\varepsilon}\tilde{\sigma}_{\mathrm{o}} & \frac{1}{\varepsilon}\tilde{R}_{\mathrm{o}} & \frac{1}{\varepsilon}\tilde{R}_{\mathrm{o}} \\ -\frac{1}{\mu}\tilde{R}_{\mathrm{e}} & -\frac{1}{\mu}\tilde{R}_{\mathrm{e}} & -\frac{1}{\varepsilon}R\tilde{\sigma}_{\mathrm{e}} & \tilde{0} \\ -\frac{1}{\mu}\tilde{R}_{\mathrm{o}} & -\frac{1}{\mu}\tilde{R}_{\mathrm{o}} & \tilde{0} & -\frac{1}{\varepsilon}\tilde{\sigma}_{\mathrm{o}} \end{pmatrix} \tag{17}$$

$\tilde{\Re}_{\mathrm{T}}$ is split into two operators to derive ADI-FDTD scheme and the operators $\tilde{A}$ and $\tilde{B}$ are given by

$$\tilde{A}=\begin{pmatrix} -\frac{1}{2\varepsilon}\tilde{\sigma}_{\mathrm{e}} & \tilde{0} & \frac{1}{\varepsilon}\tilde{R}_{\mathrm{e}} & \frac{1}{\varepsilon}\tilde{R}_{\mathrm{e}} \\ \tilde{0} & -\frac{1}{2\varepsilon}\tilde{\sigma}_{\mathrm{o}} & \tilde{0} & \tilde{0} \\ \tilde{0} & \tilde{0} & -\frac{1}{2\varepsilon}\tilde{\sigma}_{\mathrm{e}} & \tilde{0} \\ -\frac{1}{\mu}\tilde{R}_{\mathrm{o}} & -\frac{1}{\mu}\tilde{R}_{\mathrm{o}} & \tilde{0} & -\frac{1}{2\varepsilon}\tilde{\sigma}_{\mathrm{o}} \end{pmatrix}$$

and

$$\tilde{B}=\begin{pmatrix} -\frac{1}{2\varepsilon}\tilde{\sigma}_{\mathrm{e}} & \tilde{0} & \tilde{0} & \tilde{0} \\ \tilde{0} & -\frac{1}{2\varepsilon}\tilde{\sigma}_{\mathrm{o}} & \frac{1}{\varepsilon}\tilde{R}_{\mathrm{o}} & \frac{1}{\varepsilon}\tilde{R}_{\mathrm{o}} \\ -\frac{1}{\mu}\tilde{R}_{\mathrm{e}} & -\frac{1}{\mu}\tilde{R}_{\mathrm{e}} & -\frac{1}{2\varepsilon}\tilde{\sigma}_{\mathrm{e}} & \tilde{0} \\ \tilde{0} & \tilde{0} & \tilde{0} & \frac{1}{2\varepsilon}\tilde{\sigma}_{\mathrm{o}} \end{pmatrix} \tag{18}$$

Compared to the unsplit-field PML scheme, the split-field PML equation is less complicate and more straightforward. However, this formulation suffers from large reflection error, when attempting to absorb the low-frequency evanescent wave. The CFS PML scheme can accurately absorb the low-frequency wave and is discussed below.

2.3. CFS PML Scheme

The PML equations can be expressed in the stretched coordinate space [7]. For example, considering the x-projection of Ampere's law

TABLE 1 Eigenvalues of Λ and G for Unsplit PML Scheme

	CFLN=1	CFLN=5	CFLN=15
Split-field PML for	9.9422334 e −001	9.9590080 e −001	1.0066924 e +000
ADI-FDTD σ=0.1066$\lvert\lambda_{\Lambda}$	9.9422334 e −001	9.9590080 e −001	1.0066924 e +000
	9.9422334 e −001	9.9590080 e −001	1.0066924 e +000
	9.9422334 e −001	9.9590080 e −001	1.0066924 e +000
	9.8563297 e −001	9.4176082 e −001	8.3275850 e −001
	9.8563297 e −001	9.4176082 e −001	8.3275850 e −001
	9.8563297 e −001	9.4176082 e −001	8.3275850 e −001
	9.8563297 e −001	9.4176082 e −001	8.3275850 e −001
	1.0000000 e +000	1.0000000 e +000	9.9999972 e −001
	9.9999999 e −001	1.0000000 e +000	1.0000000 e +000
	1.0000000 e +000	9.9999996 e −001	1.000000 e +000
	1.0000000 e +000	9.9999999 e −001	9.9999999 e −001
Split-field PML for	9.9614053 e −001	9.9851056 e −001	9.9948561 e −001
CN-FDTD σ=0.1066$\lvert\lambda_{\mathrm{G}}$	9.9614053 e −001	9.9851056 e −001	9.9948561 e −001
	9.9614053 e −001	9.9851056 e −001	9.9948561 e −001
	9.9614053 e −001	9.9851056 e −001	9.9948561 e −001
	9.8468627 e −001	9.2575790 e −001	7.9378279 e −001
	9.8468627 e −001	9.2575790 e −001	7.9378279 e −001
	9.8468627 e −001	9.2575790 e −001	7.9378279 e −001
	9.8468627 e −001	9.2575790 e −001	7.9378279 e −001
	1.0000000 e +000	1.0000000 e +000	9.9999986 e −001
	1.0000000 e +000	1.0000000 e +000	9.9999996 e −001
	9.9999999 e −001	9.9999996 e −001	1.000000 e +000
	1.0000000 e +000	9.9999998 e −001	1.0000000 e +000

$$j\omega\varepsilon E_x = \frac{1}{s_y}\frac{\partial}{\partial y}H_z - \frac{1}{s_z}\frac{\partial}{\partial_z}H_y \tag{19}$$

and the z-projection of Faraday's law

$$j\omega\mu H_z = \frac{1}{s_y}\frac{\partial}{\partial y}E_x - \frac{1}{s_x}\frac{\partial}{\partial_x}E_y \tag{20}$$

where s_i is the stretched coordinate metric and is chosen to be

$$s_i = \kappa_i + \frac{\sigma_i}{\alpha_i + j\omega\varepsilon} \tag{21}$$

When (19) and (20) are transformed into time-domain, the right-hand side terms will become convolution. The convolutional CFS PML scheme is not suitable to formulate CN-FDTD method. In [10], the authors use the auxiliary differential equations to express the Eqs. (16) and (17) and formulate CFS PML scheme to be suitable for CN-FDTD scheme. The field vector is defined as

$$\begin{aligned}\vec{\Psi} = (&E_x \quad E_y \quad E_z \quad f_{xy} \quad f_{xz} \quad f_{yz} \quad f_{yx} \quad f_{zx} \quad f_{zy} \\ &H_x \quad H_y \quad H_z \quad g_{xy} \quad g_{xz} \quad g_{yz} \quad g_{yx} \quad g_{zx} \quad g_{zy})\end{aligned} \tag{22}$$

where f and g are auxiliary variables and $\tilde{\Re}_T$ is a 18 × 18 dimensional space operator

$$\tilde{\Re}_T = \begin{pmatrix} \tilde{0} & \frac{1}{\varepsilon}\tilde{C}_{ss} & \frac{1}{\varepsilon}\tilde{R}_k & \tilde{0} \\ \tilde{0} & -\tilde{\sigma}_s & \tilde{R}_{ss} & \tilde{0} \\ -\frac{1}{\mu}\tilde{R}_k & \tilde{0} & \tilde{0} & -\frac{1}{\mu}\tilde{C}_{ss} \\ \tilde{R}_{ss} & \tilde{0} & \tilde{0} & -\tilde{\sigma}_s \end{pmatrix} \tag{23}$$

After splitting $\tilde{\Re}_T$, we can derive the ADI-FDTD scheme. The operators $\tilde{A}$ and $\tilde{B}$ are given by

$$\tilde{A} = \begin{pmatrix} \tilde{0} & \frac{1}{\varepsilon}\tilde{C}_{se} & \frac{1}{\varepsilon}\tilde{R}_{ke} & \tilde{0} \\ \tilde{0} & -\frac{1}{2}\tilde{\sigma}_s & \tilde{R}_{sse} & \tilde{0} \\ \frac{1}{\mu}\tilde{R}_{ko} & \tilde{0} & \tilde{0} & -\frac{1}{\mu}\tilde{C}_{so} \\ \tilde{R}_{sso} & \tilde{0} & \tilde{0} & -\frac{1}{2}\tilde{\sigma}_s \end{pmatrix}$$

and

$$\tilde{B} = \begin{pmatrix} \tilde{0} & \frac{1}{\varepsilon}\tilde{C}_{so} & \frac{1}{\varepsilon}\tilde{R}_{ko} & \tilde{0} \\ \tilde{0} & -\frac{1}{2}\tilde{\sigma}_s & \tilde{R}_{sso} & \tilde{0} \\ -\frac{1}{\mu}\tilde{R}_{ke} & \tilde{0} & \tilde{0} & -\frac{1}{\mu}\tilde{C}_{se} \\ \tilde{R}_{sse} & \tilde{0} & \tilde{0} & -\frac{1}{2}\tilde{\sigma}_s \end{pmatrix} \tag{24}$$

where $\tilde{R}_{ss} = \tilde{R}_{sse} + \tilde{R}_{sso}$, $\vec{C}_{ss} = \vec{C}_{sse} + \vec{C}_{sso}$, and $\vec{R}_k = \vec{R}_{ke} + \vec{R}_{ko}$. The matrices $\tilde{R}_{ss}$, $\vec{C}_{ss}$, and $\vec{R}_k$ are related to PML parameters κ, σ, and α. Details of these matrices are shown in [10]. The ADI-FDTD with CFS PML is a simple extension of the ADI-FDTD method. This scheme can provide wideband absorption of the incident wave.

3. THEORETICAL STABILITY ANALYSIS

To study the stability of the PML schemes for the CN-FDTD and ADI-FDTD method, the von Neumann method is used. Following the similar procedures presented in [3], we assume that for each time step the field components are Fourier-transformed into the spatial spectral domain. From the system equations of (4), the CN-FDTD scheme can be written in the spatial spectral domain in a matrix form as

$$\mathrm{X}^{n+1} = G\mathrm{X}^n \tag{25}$$

where the vector X^n represents the field components and the auxiliary variables at the nth time step. From the system equations of (7), the ADI-FDTD scheme can also be written in the spatial spectral domain in matrix form as

$$M_1\mathrm{X}^{n|} = P_1\mathrm{X}^n \tag{26}$$

$$M_2\mathrm{X}^{n+1} = P_2\mathrm{X}^{n|} \tag{27}$$

for the n^* and $n + 1$ time steps, respectively. The entries for the matrices M and P are derived from updating equations. The two half time steps can be combined to one time step

$$X^{n+1} = M_2^{-1}P_2M_1^{-1}P_1X^n = \Lambda X^n \tag{28}$$

The stability criterion requires that the eigenvalues of amplification matrices G and Λ lie within or on the unit circle. An attempt to determine the eigenvalues of G and Λ symbolically was made. However, due to the complexity of the amplification matrix, it is difficult to get a simplified analytical expression for the eigenvalues. The maximum eigenvalues are numerically calculated by Matlab®. In this study, we set the cell size to be $\Delta x = \Delta y = \Delta z = 1.0$ mm and FDTD time step limit $\Delta t\max = 1.92$ ps is used. The ratio of $\Delta t/\Delta t\max$ is defined as the CFLN.

3.1. Unsplit-Field PML Scheme

The eigenvalues of G and Λ are computed when $\sigma_x = \sigma_z = 0$, and $\sigma_y = 10.66$ S/m. The time step sizes are chosen to be $\Delta t_{\max}$, $2\Delta t_{\max}$, and $5\Delta t_{\max}$, respectively. Both the unsplit-field PML schemes for the CN-FDTD scheme and ADI-FDTD are investigated and the theoretical results are shown in Table 1. When CFLN = 1, both the ADI-FDTD and CN-FDTD PML formulations can be stable as the maximum eigenvalues for the two schemes are smaller than unity. However, it is found that the eigenvalues of the unsplit-field PML scheme for ADI-FDTD scheme are larger than unity when CFLN = 2 is used. Conversely, we use different CFLN and σ values and no instability was observed for CN-FDTD PML scheme. As shown in (5), the difference between CN-FDTD and ADI-FDTD is the Δt^2 perturbation term. The results indicate that perturbation term will affect the stability of PML scheme for ADI-FDTD when large CFLN is used.

3.2. Split-Field PML Scheme

The split-field PML schemes for CN-FDTD and ADI-FDTD are studied. In [9], it indicated that the split-field PML for the ADI-FDTD method will be unstable when the PML conductivity

TABLE 2 Eigenvalues of Λ and G for Split PML Scheme

	CFLN=1	CFLN=2	CFLN=5
Unsplit-field PML for	1.0000000 e +000	1.0000000 e +000	1.0000000 e +000
ADI-FDTD $\sigma=10.66\|\lambda\|$	8.7747147 e −001	1.0000000 e +000	1.0000000 e +000
	8.7747147 e −001	1.1404158 e +000	1.8425689 e +000
	8.7747147 e −001	1.1404158 e +000	1.8425689 e +000
	1.0000000 e +000	1.0000000 e +000	1.8425689 e +000
	1.0000000 e +000	1.0000000 e +000	1.8425689 e +000
	8.7747147 e −001	1.1404158 e +000	1.0000000 e +000
	3.0475086 e −001	1.1404158 e +000	1.0000000 e +000
	3.0475086 e −001	4.3679841 e −001	4.1123514 e −001
	3.0475086 e −001	4.3679841 e −001	4.1123514 e −001
	3.0475086 e −001	4.3679841 e −001	4.1123514 e −001
	1.0000000 e +000	4.3679841 e −001	4.1123514 e −001
Unsplit-field PMLfor	1.0000000 e +000	1.0000000 e +000	1.0000000 e +000
CN-FDTD $\sigma=10.66\|\lambda_G\|$	9.2402257 e −001	9.2903235 e −001	9.6195689 e −001
	9.2402257 e −001	9.2903235 e −001	9.6195689 e −001
	9.2402257 e −001	9.2903235 e −001	9.6195689 e −001
	9.2402257 e −001	9.2903235 e −001	9.6195689 e −001
	2.3259772 e −001	4.6207853 e −001	7.3695418 e −001
	2.3259772 e −001	4.6207853 e −001	7.3695418 e −001
	2.3259772 e −001	4.6207853 e −001	7.3695418 e −001
	2.3259772 e −001	4.6207853 e −001	7.3695418 e −001
	1.0000000 e +000	1.0000000 e +000	1.0000000 e +000
	1.0000000 e +000	9 9999998 e −001	9.9999997 e −001
	1.0000000 e +000	1.0000000 e +000	1.0000000 e +000

profile is polynomial scaled and this scheme can be stable with constant PML conductivity. In this study, the smaller PML conductivity $\sigma_x = \sigma_z = 0$ and $\sigma_y = 0.1066$ S/m is used. From Table 2, it is found that the split-field PML scheme for ADI-FDTD can be stable when CFLN = 5 and will become unstable when large CFLN = 15 is used. No instability is observed when split-field PML for CN-FDTD scheme is used.

3.3. CFS PML Scheme

The convolutional CFS PML scheme is not suitable to formulate CN-FDTD method. It has also been proved in [7] that convolutional CFS PML for ADI-FDTD can be unconditionally stable. In [10], the CFS PML formulations can also be expressed for CN-FDTD and ADI-FDTD schemes, as discussed in Section 2. We find that the CFS PML for CN-FDTD can still be unconditionally stable. Table 3 shows the calculated eigenvalues of Λ with $\sigma_s = 10$ S/m, $\kappa_s = 5$, and $\alpha_s = 0.1$ S/m. When CFS PML is formulated for ADI-FDTD (7), this scheme will also lead to unstable condition when large CFLN = 15 is used.

4. NUMERICAL VERFICATION

Numerical simulations are performed by 3-D ADI-FDTD with unsplit-field PML and split-field PML to validate the instability of the two schemes. A uniform mesh with cell size $\Delta x = \Delta y = \Delta z = 1.0$ mm and FDTD time step limit $\Delta t_{max}=1.92$ ps are used. The computation domain is $42 \times 42 \times 42$. PML layers that are 10 cells thick terminated all six sides of the computation domain. A differential Gaussian pulse applied to H_x field is excited at the center position (21, 21, 21). The polynomial scaling is used for the PML conductivity profile

TABLE 3 Eigenvalues of Λ for CFS PML ADI-FDTD with ADE Formulation

	CFLN=1	CFLN=5	CFLN=15
Unsplit-field PML	6.4610024 e −001	9.5826739 e −001	6.7860023 e −001
for ADI-FDTD $\|\lambda_\Lambda\|$	6.4610024 e −001	9.5826739 e −001	6.7860023 e −001
	6.4610024 e −001	9.5826739 e −001	6.7860023 e −001
	6.4610024 e −001	9.5826739 e −001	6.7860023 e −001
	6.3629102 e −001	1.0000000 e +000	1.1340967 e +000
	9.9044985 e −001	1.0000000 e +000	1.1340967 e +000
	9.9044985 e −001	2.4086514 e −001	1.1340967 e +000
	9.9044985 e −001	2.4086514 e −001	1.1340967 e +000
	9.9044985 e −001	2.4086514 e −001	1.0000000 e +000
	1.0000000 e +000	2.4086514 e −001	1.0000000 e +000
	1.0000000 e +000	1.6715028 e −001	4.0697273 e −001
	6.3629102 e −001	1.6715028 e −001	4.0697273 e −001
	6.3629102 e −001	1.2104686 e −001	4.0697273 e −001
	6.3629102 e −001	1.2104686 e −001	4.0697273 e −001
	6.3267285 e −001	1.6715028 e −001	2.1521203 e −001
	6.3267285 e −001	1.6715028 e −001	2.1521203 e −001
	6.3267285 e −001	1.2104686 e −001	2.1521203 e −001
	6.3267285 e −001	1.2104686 e −001	2.1521203 e −001

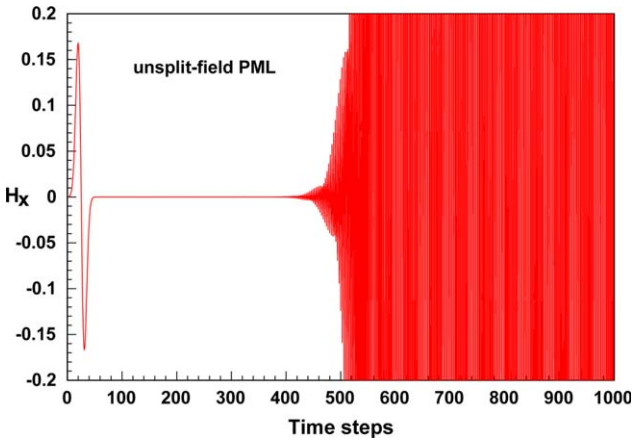

Figure 1 The H_x component for ADI-FDTD with unsplit-field PML (CFLN = 2). [Color figure can be viewed in the online issue, which is available at wileyonlinelibrary.com]

$$\sigma_{s\max}=\sigma_{\text{opt}}\approx\frac{(m+1)}{150\pi\Delta s}$$
$$\sigma_s(s)=\frac{\sigma_{s\max}|S-S_0|^m}{d_m}\quad s=x,y,z \tag{29}$$

where d is the thickness of PML absorber, Δs is the cell size, and s_0 represents the interface. In this simulation, we choose scaling factor $m = 4$ and $\sigma_{\max} = 10.61$ S/m for optimum PML performance [4].

First, numerical simulation of the ADI-FDTD with unsplit-field PML is performed. The time step size in this study is chosen to be $2\Delta t_{\max}$. Figure 1 shows the time-domain H_x fields recorded at the position (21, 20, 21). As shown in Figure 1, this scheme will become unstable after running 400 time steps.

Then, numerical simulation of the ADI-FDTD with split-field PML is performed. The time step size in this study is $7\Delta t$max. As shown in Figure 2, this scheme will become unstable after running 1200 time steps.

5. CONCLUSION

In this work, the stability analysis of the PML schemes for the ADI-FDTD and CN-FDTD are studied. The ADI-FDTD can be seen as a second-order perturbation of the CN-FDTD method.

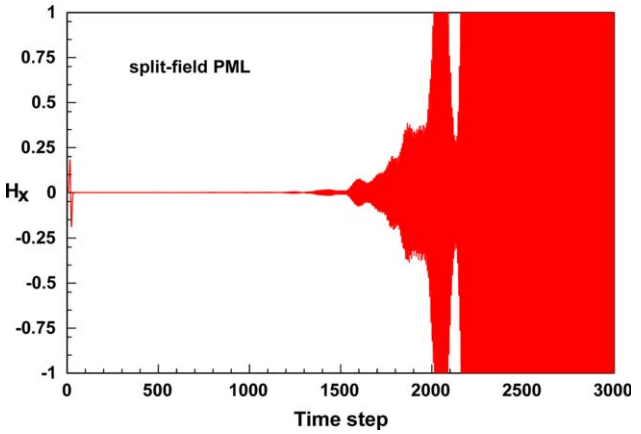

Figure 2 The H_x component for ADI-FDTD with split-field PML (CFLN = 7). [Color figure can be viewed in the online issue, which is available at wileyonlinelibrary.com]

From the theoretical stability analysis, it is found that the ADI-FDTD will be unstable while the CN-FDTD can remain stable when the PML medium is used. We find that the Δt^2 perturbation term will affect the stability of the PML schemes for ADI-FDTD.

REFERENCES

1. A. Taflove and S. Hagness, Computational electrodynamics: the finite-difference time-domain method, 3rd ed., Artech House, Boston, MA, 2005.
2. T. Namiki, A new FDTD algorithm based on alternating-direction implicit method, IEEE Trans Microwave Theory Tech 47 (1999), 2003–2007.
3. F. Zheng, Z. Chen, and J. Zhang, Toward the development of a three-dimensional unconditionally stable finite-difference time-domain method, IEEE Trans Microwave Theory Tech 48 (2000), 1550–1558.
4. G. Liu and S.D Gedney, Perfectly matched layer media for an unconditionally stable three-dimensional ADI-FDTD method, IEEE Microwave Guided Wave Lett 10 (2000), 261–263.
5. C.C.-P. Chen, T.-W. Lee, N. Murugesan, and S.C. Hagness, Generalized FDTD-ADI: An unconditionally stable full-wave Maxwell's equations solver for VLSI interconnect modeling, In: Proceedings of International Conference on Computer-Aided Design, San Jose, CA, 2000, pp. 156–163.
6. R.G. Rubio, S.G. Garcia, A.R. Bretones, and R.G. Martin, An unsplit Berenger-Like PML for the ADI-FDTD method, Microwave Opt Technol Lett 42 (2004), 466–469.
7. S.D. Gedney, G. Liu, J.A. Roden, and A. Zhu, Perfectly matched layer media with CFS for an unconditionally stable ADI-FDTD method, IEEE Trans Antennas Propag 49 (2001), 1554–1559.
8. L. Wang and C. Liang, A new implemenetation of CFS-PML for ADI-FDTD method, Microwave Opt Technol Lett 49 (2006), 1924–1928.
9. J.-N. Hwang and F.-C. Chen, A modified PML conductivity profile for the ADI-FDTD Method with split-field PML, IET Proc Microwave Antennas Propag 1 (2007), 1071–1077.
10. R.G. Rubio, S.G. Garcia, A.R. Bretones, and R.G. Martin, Crank-Nicolson reformulation of ADI-FDTD PML extensions, Antennas Wireless Propag Lett 5 (2006), 357–360.
11. D. Wu and J. Chen, Perfectly matched layer for Crank-Nicolson (CN) FDTD method, In IEEE Antennas Propagation Symposium. Digest, Monterey, CA, 2004, pp. 583–586.
12. O. Ramadan. Unconditionally stable Crank-Nicolson nearly PML algorithm for truncating linear Lorentz dispersive FDTD domains, IEEE Trans Microwave Theory Tech 54 (2006), 2807–2812.

REFRACTIVE INDEX SENSOR BASED ON MACH–ZEHNDER INTERFEROMETER FORMED BY TWO CASCADED SINGLE MODE FIBER CORNERS

Qingguo Shi,[1,2] Daru Chen,[1,2] Xiaogang Jiang,[1,2] Baojin Peng,[1,2] and Xueqin Lei[1,2]
[1] Institute of Information Optics, Zhejiang Normal University, Jinhua 321004, China; Corresponding author: daru@zjnu.cn
[2] Joint Research Laboratory of Optics of Zhejiang Normal University and Zhejiang University, Jinhua 321004, China

Received 19 March 2014

ABSTRACT: *We reported a novel fiber sensor based on two cascaded single mode fiber corners, which has a high sensitivity for refractive index (RI) sensing and a low temperature crosstalk. RI sensing was experimentally demonstrated with an average sensitivity of 235 nm/RI*